Phys Chem Minerals (2002) 29: 240–253
DOI 10.1007/s00269-001-0232-4

ORIGINAL PAPER

A. M. Seydoux-Guillaume · R. Wirth · L. Nasdala
M. Gottschalk · J. M. Montel · W. Heinrich

An XRD, TEM and Raman study of experimentally annealed natural monazite

Received: 7 May 2001 / Accepted: 11 October 2001

Abstract The healing of radiation damage in natural monazite has been experimentally studied in annealing experiments using XRD, TEM, Raman microprobe and cathodoluminescence analysis. The starting material was a chemically homogeneous monazite from a Brazilian pegmatite with a concordant U–Pb age of 474 ± 1 Ma and a U–Th/He age of 479 Ma. The monazite shows nm-scale defects induced by radioactive decay. The X-ray pattern of the unheated starting material revealed two distinct monazite "phases" A and B with slightly different lattice parameters. Monazite A shows sharp reflections of high amplitudes and slightly expanded lattice parameters (1% in volume) compared to a standard monazite. Phase B exhibits very broad reflections of low amplitudes. Two sets of experiments were performed. First, dry monazite powder was annealed at 500, 800 and 1000 °C for 7 days. Each run product was analysed by X-ray diffractometry. Second, monazite grains were hydrothermally annealed at temperatures from 500 to 1200 °C for 5 to 15 days. TEM observations show that partial healing of the monazite lattice already occurred at 500 °C and increased gradually with temperature, so that after 10 days at 900 °C complete healing was achieved. The observations are interpreted accordingly: the starting material has a mosaic structure consisting of two domains, A and B, which are basically two monazite crystals with different lattice parameters. We suggest that the A domains correspond to well-crystallised areas where helium atoms are trapped. The accumulation of He causes expansion of the A monazite lattice. Diffraction domains B are interpreted as a helium-free distorted monazite crystal lattice, which can be referred to old alpha-recoil tracks. These B domains are composed of "islands" with an expanded lattice, induced by the presence of interstitials, and "islands" of a compressed monazite lattice, induced by presence of vacancies. Both the islands will pose stress on the lattice in the vicinity of the islands. The broadening of the B reflections is due to the expanded or compressed diffraction domains and to the different amount of the distortion.

With increasing temperature the unit-cell volume of monazite A decreases, i.e. the position of the A reflections shifts towards smaller d_{hkl} values. This was interpreted as a relaxation of the monazite lattice due to helium diffusion out of the monazite lattice. Simultaneously, the nm-sized defect domains B are healed. At 900–1000 °C only a monazite with well-crystallised lattice and minimum unit-cell volume is observed.

Keywords Monazite · Annealing experiments · Helium · XRD · TEM

A. M. Seydoux-Guillaume (✉) · R. Wirth · M. Gottschalk
W. Heinrich
GFZ-Potsdam-Division 4, Telegrafenberg,
14473 Potsdam, Germany

L. Nasdala
Institut für Geowissenschaften – Mineralogie,
Johannes Gutenberg-Universität, 55099 Mainz, Germany

J. M. Montel
LMTG-UMR 5563,
Laboratoire de Minéralogie Université Paul Sabatier,
39 Allées Jules Guesde, 31000 Toulouse, France

Present address:
A. M. Seydoux-Guillaume
Institut für Planetologie
Wilhelm-Klemm-Str.10
48149 Münster, Germany
e-mail: seydoux@uni-muenster.de
Tel: +49-251-83 33 405

Introduction

Monazite, the natural light rare-earth orthophosphate, is widely used in U–Th–Pb geochronology (Parrish 1990) because of its high actinide content (up to 6 wt% UO_2 and up to 20 wt% ThO_2). In contrast to zircon, monazite is mostly concordant in a U–Pb concordia diagram (Schärer et al. 1986; Corfu 1988; Smith and Barreiro 1990; Landzirotti and Hanson 1995; Parrish 1995), meaning that during most geological events the monazite U–Pb system is either completely reset or remains totally unaffected. Nevertheless, discordant U–Pb ages have also been reported; mostly, they reflect a mixture of newly grown rims with inherited cores (Cocherie et al. 1998; Paquette et al. 1999; Krohe and Wawrzenitz 2000) and rarely a diffusive Pb loss (Suzuki and Adachi 1994; Suzuki et al. 1994). To understand the significance of the U–Pb ages measured from monazite samples, one needs to understand the mechanism of U–Pb resetting.

Two processes are commonly considered to explain the resetting of the U–Pb isotopic system: Pb loss by volume diffusion out of the grain or dissolution of the crystal via a coexisting fluid and precipitation of a new-formed Pb-free crystal (Teufel and Heinrich 1997; Seydoux et al. 1999). Dodson (1973) investigated the resetting by diffusion theoretically. In this model, resetting results from the diffusion of the daughter isotopes out of the crystal. This model introduces the concept of a closure temperature, which depends on the size of the crystal, its shape, the cooling rate during the geological event and the diffusion coefficient of the daughter elements. For example, in a metamict crystal, Pb is able to diffuse relatively fast along the interfaces between amorphous and crystalline domains in comparison to the diffusion in the amorphous and in the crystalline domains themselves (Cherniak et al. 1991; Cherniak 1993; Murakami et al. 1991; Salje 2000; Weber et al. 1998). The proposed resetting by a dissolution–precipitation mechanism is based on the dissolution of the crystal in a melt or in a fluid phase, followed by a reprecipitation of a newly formed crystal without reincorporation of the daughter element. No detailed model for dissolution precipitation resetting is available, but we predict the kinetics of dissolution, the solubility of the crystal and the nature of the fluid phase to be important parameters.

In minerals relevant for U–Th–Pb dating, the radioactive decay produces also radiation damage that may partially or totally destroy the crystal lattice, thus producing a so-called metamict crystal. Whatever the mechanism of resetting is considered to be, it can be anticipated that the kinetics of resetting will be strongly influenced by the degree of metamictization of the crystal.

Previous studies on metamictization

The monazite studied in the present work contains 1300 ppm UO_2 and 69 000 ppm ThO_2; its composition is given in Table 1. The U and Th radioactive decay produces α-particles (^{4}He nuclei), until Pb is finally created. During an α-event, a heavy atom nucleus liberates its energy by ejecting an α-particle to about 10–40 μm (Owen 1988; Ewing et al. 1995; Ewing et al. 2000; Nasdala et al. 2001b) from the point of disintegration. It dissipates most of its energy by ionisation along its path, with limited elastic collisions occurring at the end of its trajectory (Nasdala et al. 2001a) and produces isolated defects (several hundred atomic displacements). In contrast, the remaining nucleus is recoiled in an opposite direction, to about 10–20 nm, from the α-particle, according to the principle of momentum conservation, and causes collision cascades (a few thousand atomic displacements) (Gögen and Wagner 2000; Nasdala et al. 2001b). Most of the atomic displacements leading to amorphisation of a crystal lattice are caused by alpha-recoil nuclei (Ewing et al. 1995, 2000; Nasdala et al. 1996; Weber et al. 1998).

Table 1 Electron microprobe (EMP) analyses of starting monazite Moacir. The data represent an average of 30 analyses of a 400-μm diameter single grain. Cations per formula unit are calculated on the basis of 16 oxygens. The operating conditions were given in Förster (1998)

Oxides	wt%	Cations
La_2O_3	14.51	0.860
Ce_2O_3	30.59	1.799
Pr_2O_3	3.14	0.184
Nd_2O_3	10.20	0.585
Sm_2O_3	2.05	0.114
Gd_2O_3	0.94	0.050
Dy_2O_3	0.11	0.006
Er_2O_3	0.05	0.002
SiO_2	1.42	0.229
Y_2O_3	0.71	0.061
P_2O_5	27.81	3.782
CaO	0.44	0.076
ThO_2	6.92	0.253
UO_2	0.13	0.005
PbO	0.16	0.007
Total	99.19	8.011

In contrast to zircon (Speer 1982), monazite is almost never found in the metamict state (Ewing 1975), despite the fact that monazite incorporates large quantities of U and Th, thus receiving intensive radiation doses during its geologic history. Clear evidence for radiation damage in natural monazite is limited to isolated domains within the crystal (Black et al. 1984; Meldrum et al. 1998). This suggests that, even at low temperature, the monazite lattice is healed easily (Boatner and Sales 1988).

Radiation damage in minerals can also be induced by using external heavy-ion irradiation. For most crystals it is possible to define an amorphization dose above which the crystal is totally metamict (amorphous state). The amorphization dose increases with increasing temperature and reaches a critical temperature above which amorphization can no longer be achieved, because the crystal lattice is thermally reconstructed faster than it is destroyed.

The results of irradiation studies carried out on silicates and phosphates with monazite or zircon structure can be summarised as follows. At room temperature, the amorphisation dose is similar for all the investigated structures. It shows that monazite is not specifically resistant to radiation damages. The main difference is the critical temperature, which for monazite is in the range of 100 to 200 °C, but lies for zircon above 1000 °C (Meldrum et al. 1996, 1997, 1998, Meldrum et al. 1999, 2000). Therefore, monazite is able to restore its structure at low temperature, although it is not specifically resistant to radiation damage.

Previous works on the annealing of monazite provided different results. Karioris et al. (1981) in a X-ray diffraction (XRD) study on artificially amorphized synthetic monazite powder, and Meldrum et al. (1998) in a transmission electron microscopy (TEM) study on artificially amorphized natural monazite, observed recrystallization at 300 and 450 °C, respectively. In contrast, in an XRD study, Smith and Giletti (1997) completely healed a natural monazite only between 800 and 1100 °C.

This paper presents the results of annealing experiments using a natural monazite. Using XRD and TEM [high-resolution transmission electron microscopy (HRTEM) and dark field (DF)], the annealing of radiation damages was evaluated. The experimental work is completed by first attempts to document the structural recovery of annealed monazites by Raman spectroscopic and CL (cathodoluminescence) analyses. Implications of our results for U–Pb geochronology and nuclear waste storage are discussed.

Experimental

Starting material

A yellow-orange single crystal of monazite (3 × 2 cm in size) from a Brazilian pegmatite (Cruz et al. 1996) was used for this study (Moacir monazite). Scanning electron microscopy and optical microscopy observations showed that the crystal is almost free of inclusions. The crystal is homogeneous on the micron scale and contains about 1300 ppm of U, 69 000 ppm of Th and 1600 ppm of Pb (Table 1).

The crystal has concordant U–Pb age of 474 ± 1(2σ) Ma (Seydoux et al. 1999). From the Pb, U and Th content and the age, a time-integrated α-dose of about 2.43×10^{16} α/mg is calculated, which corresponds to about 2 dpa (displacements per atom).

Previous X-ray diffraction patterns obtained with Si as an internal standard showed that the starting material is well crystallised, and the following cell parameters were derived: $a = 6.815(1)$ Å, $b = 7.021(1)$ Å, $c = 6.496(1)$ Å, $\beta = 103.91(1)°$ (Seydoux et al. 2000).

Annealing experiments

Dry and wet annealing experiments were performed. Dry annealing was carried out by heating powdered monazite at different temperatures and run durations, in order to study the evolution of XRD patterns with temperature and time. The starting monazite was crushed in an agate mortar into a powder with a grain size in the range of < 1 μm to 20 μm (Fig. 1a). About 20 mg of this powder was heated for 7 days at 500, 800 and 1000 °C in a platinum crucible using a chamber furnace Heraeus K1252 (Table 2). In order to investigate the kinetics of annealing, experiments at 500 and 800 °C were performed for different run durations (Table 2). Subsequently, the run products were prepared for X-ray powder diffraction investigations.

Single fragments of the starting monazite with a grain size of 200–400 μm were heated hydrothermally, in order to study the evolution of the lattice healing with temperature. After abrasion by compressed air (1.15 bar, 20 h) well-rounded grains free of inclusions and impurities (Fig. 1b) were selected under the binocular for the experiments (Seydoux et al. 1999). Ten grains were placed in a platinum capsule together with 20 μl of ultrapure water. The capsules (15 × 3 × 0.2 mm) were sealed by welding and checked for leaks by heating them at 110 °C for 24 h. The experiments were carried out in standard cold seal hydrothermal pressure vessels at 2 kbar and 500 and 800 °C and in an internally heated pressure vessel at 7 kbar and 900, 1000 and 1200 °C (Table 2). Run durations were about 10 days. Maximum error in the temperature measurements was ± 10 °C. At the end of each run, the vessels were quenched to room temperature within a few minutes. Run products were washed with ultrapure water and prepared for TEM.

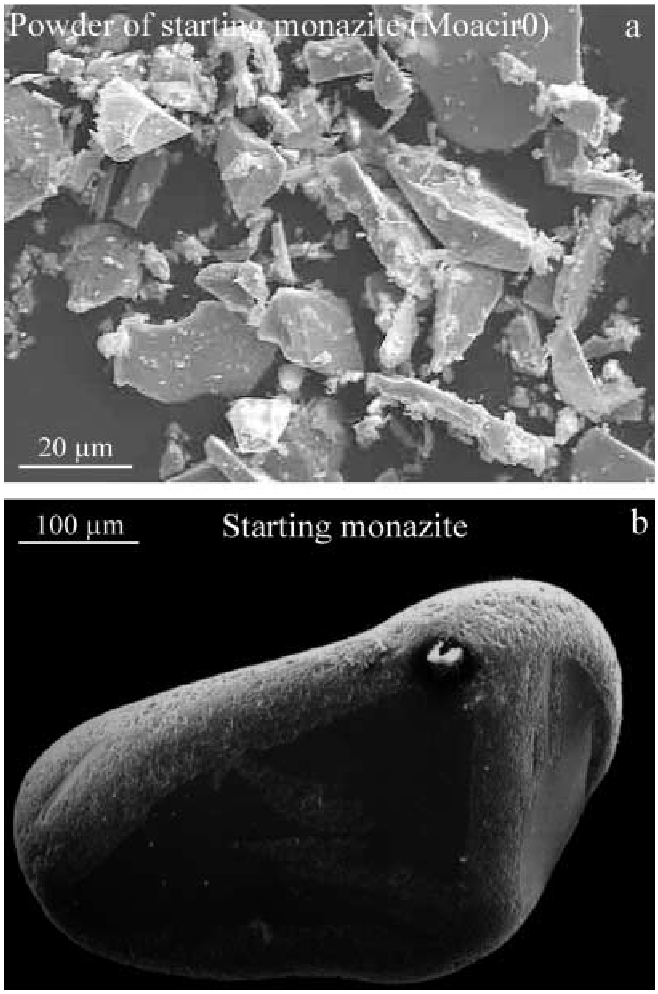

Fig. 1a, b SEM micrographs illustrating textural characteristics observed in unheated monazite. **a** Powder of monazite grains. **b** An abraded monazite grain

Analytical methods

XRD

One mg of each powder of monazite was measured in transmission mode using a fully automated STOE STADI P diffractometer (Cu–Kα_1 radiation) equipped with a primary monochromator and a 7°-position sensitive detector (PSD) (at the GFZ, Potsdam). The spectra were recorded in the range of 5–125 (2θ) using a step interval of 0.1°. The resolution of the PSD was set to 0.02°. Counting time was set to 135 s per detector step. Peak positions were calibrated externally using the NBS SRM-640b silicon standard. The unit-cell refinements were performed using the Rietveld-refinement program of the GSAS software package (Larson and Von Dreele 1988). Additional XRD patterns were recorded for all samples in

Table 2 Experimental conditions of annealing experiments with the Moacir monazite

Run	Description	Temperature (°C)	Pressure (bar)	Duration (days)
VRM97-1	Single grain	500	1000	12
VRM97-2	”	800	”	15
VRM98-1	”	900	7000	10
VRM97-10	”	1000	”	7
VRM97-6	”	1200	”	5
Mo500-24	Powder	500	1	1
Mo500-48	”	”	”	2
Mo500-72	”	”	”	3
Mo500-96	”	”	”	4
Mo500120	”	”	”	5
Mo500-6d	”	”	”	6
Mo500-7d	”	”	”	7
Mo50014d	”	”	”	14
Mo50030d	”	”	”	30
Mo800-7d	Powder	800	1	7
Mo80014d	”	”	”	14
Mo80021d	”	”	”	21
Mo80030d	”	”	”	30
Mo10007d	Powder	1000	1	7

the range of 26–28° (2θ), which corresponds to the position of the (200) reflection of the monazite. Counting time was set to 1000 s per detector step. XRD patterns in the range of 26–28° (2θ) were fitted by a Gauss + Lorentz area function, in order to measure the full width at half maximum (FWHM), amplitudes, areas and diffraction maximum positions of the (200) reflection.

TEM

The single crystals were cut in random orientation and TEM foils were prepared by hand polishing and ion milling at 5 kV. The TEM studies were carried out using the Philips CM 200 TEM of the GFZ, Potsdam operated at 200 kV using an LaB_6 electron source. HRTEM images were acquired as energy-filtered images applying a 10-eV window to the zero-loss peak using a Gatan GIF^{TM} system.

Raman analysis

Raman spectra were obtained using a Renishaw RM 1000 (in Vienna), which is a notch filter-based Raman spectrometer equipped with Leica DMLM optical microscope and Peltier-cooled CCD (charge-coupled device) detector. He–Ne 632.8 nm (3 mW) excitation was used. Measurements were done with a Leica 50× objective (numerical aperture 0.75). A grating with 1200 grooves mm^{-1} was used, resulting in an effective spectral resolution (apparatus function) of 3 cm^{-1}. For more experimental details see Nasdala and Massonne (2000). Previous Raman measurements had shown that the full width at half maximum (FWHM) of the $\nu_1(PO_4)$ Raman band, which is used to monitor the degree of short-range order, shows no significant orientational dependence (Nasdala et al. 1999). Therefore, the polished monazite samples (prepared in microprobe mounts with random crystallographic orientation) were oriented under the Raman microscope to obtain a high $\nu_1(PO_4)$ Raman band signal.

Cathodoluminescence

CL images of monazites were taken using a JEOL JXA 8900 RL electron microprobe (in Göttingen). The voltage was set to 20 kV with a beam current of 50 nA. As the absolute CL signal intensity emitted from a sample is most strongly affected by the experimental conditions, samples to be compared were brought simultaneously in the vacuum chamber and analysed under identical size of scanned area and constant signal amplification and exposure time. Although conclusions from the absolute intensities of the CL emission are rather limited, a relative comparison of intensities is possible between images taken of the same analysis run.

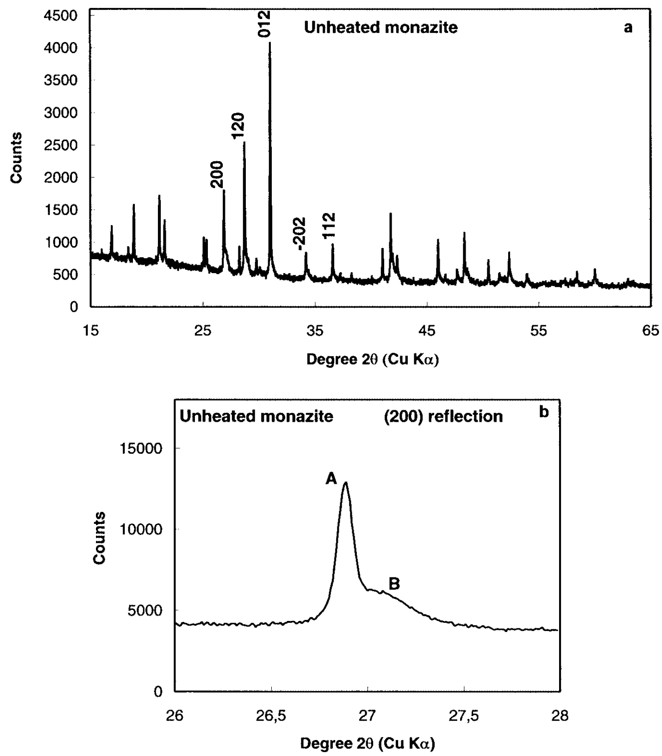

Fig. 2 a X-ray powder diffraction pattern of the unheated monazite. Note the broadening of the reflections, indicating a distortion of the monazite lattice. **b** X-ray powder diffraction pattern of the unheated monazite [26–28° (2θ)]. We distinguish two phases *A* and *B*. *A* shows a sharp reflection (FWHM = 0.091) with high amplitude. *B* exhibits very broad reflection (FWHM = 0.425) with low amplitude

Results

X-ray diffraction analysis

Unheated monazite

The diffraction pattern of unheated monazite (Fig. 2a) shows sharp reflections of relatively high amplitudes. For some reflections a broadening at the reflection bases was observed. This broadening seems to be more pronounced along the *a* direction, e.g. the (200) reflection between 26 and 28° (2θ). A typical diffraction pattern in the range of 26–28° (2θ) of the unheated monazite is given in Fig. 2b. It shows one characteristic reflection A of high amplitude, which is very sharp (FWHM = 0.091°) and additionally a broad (FWHM = 0.425°) shoulder B of low amplitude (Table 3). The B-reflection maximum is located at a larger 2θ value of 27.04° (3.295 Å) than the A-reflection maximum, which is located at 26.88° (3.314 Å) (Table 3). The area percentage of A and B

Table 3 Unit-cell parameters (Å), FWHM (° 2θ), amplitude (counts), centre of the maximum diffraction angle (2θ) and % area for the (200) diffraction maximum (phases *A* and *B*) for the unheated monazite (Moacir 0) and for different annealing conditions

Exp. no[a]	Moacir 0[b]	Mo500-7d	Mo800-7d	Mo10007d	Moacir 0	Mo500-7d	Mo800-7d
A					B		
a	6.823(1)[c]	6.813(1)	6.801(1)	6.786(1)	6.783(5)	6.788(7)	6.773(6)
b	7.026(1)	7.019(1)	7.012(1)	7.007(1)	7.014(6)	7.001(7)	6.995(7)
c	6.499(1)	6.484(1)	6.468(1)	6.464(1)	6.489(5)	6.471(6)	6.443(6)
β	103.79(1)	103.73(1)	103.65(1)	103.57(1)	103.69(9)	103.67(10)	103.77(10)
V	302.60(9)	301.22(9)	299.78(6)	298.77(3)	299.98(36)	298.83(42)	296.48(38)
FWHM[d]	0.091(1)	0.093(1)	0.083(1)	0.092(1)	0.425(6)	0.420(14)	0.296(18)
Amplitude	7533	3436	11153	11226	2026	736	1088
Centre	26.88	26.92	26.95	27	27.04(1)	27.08(1)	27.16(1)
% Area	47.01	51.01	75.11	~100	52.99	48.99	24.89

[a] Run duration for all experiments is 7 days
[b] Moacir 0 corresponds to the unheated monazite. See Table 2 for details of the experimental conditions
[c] Numbers in brackets are 2σ errors of the last significant digits
[d] FWHM: full width at half maximum

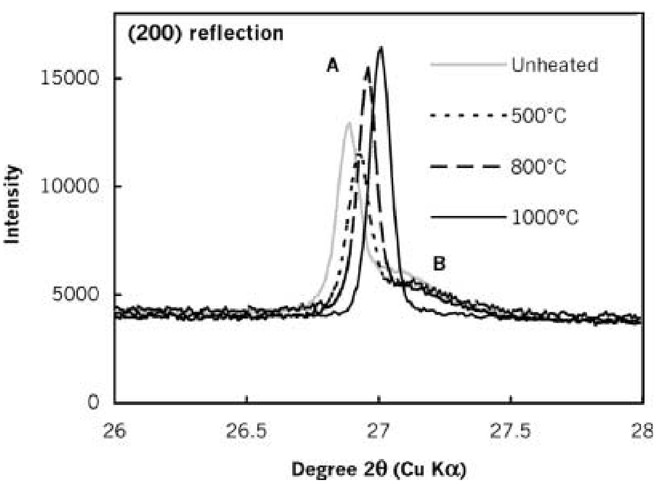

Fig. 3 X-ray powder diffraction patterns in the range of 26–28° (2θ) at different annealing conditions. We observe that the phase *B* disappears with increasing temperature and the *A* reflection shifts to higher scattering angles. At 1000 °C, X-ray diffractometry shows only one phase

reflections are 47.01 and 52.99%, respectively (Table 3). Careful examination of the whole diffraction pattern shows that this is a general feature of all reflections.

Rietveld refinement of the unheated monazite, assuming only a single phase (A) with a monazite structure, failed. However, introducing a second phase (B) also with monazite structure resulted in a successful Rietveld refinement. Consequently, the patterns were interpreted as two monazite phases with different lattice parameters (Table 3). Monazite A shows larger lattice parameters (1% in volume) than the reference crystal from Ni et al. (1995). The lattice parameters of monazite B are about the same as that of the reference.

Evolution with temperature

In order to evaluate the annealing effect on the lattice of monazite, the (200) reflections between 26 and 28° (2θ) of the unheated monazite were compared with those of the monazite heated of 500, 800 and 1000 °C (Fig. 3). A different evolution of the sharp reflection A and the broad reflection B was observed. With increasing temperature the A diffraction maximum shifts from 26.88 (3.314 Å) to 27.00° (3.300 Å) and the maximum number of counts increases from 7533 to 11 226. Annealing causes a reduction in the lattice parameters of monazite A (Table 3). However, the FWHM of A remains small and constant (≈ 0.09°). At 1000 °C, the A-lattice parameters approach those of the reference crystal (Ni et al. 1995).

With increasing temperature, the B diffraction maximum decreases in amplitude and disappears completely at 1000 °C.

Evolution with time

Figure 4 shows the evolution of the amplitude ratios of A and B reflections at 500 and at 800 °C as a function of time (ratios are given in Table 4). The significant variations of the A/(A + B) and B/(A + B) amplitude ratios were observed, either at 500 nor at 800 °C as a function of time. At 500 °C the A/(A + B) ratio is about 0.8 and the B/(A + B) ratio is 0.2, whereas at 800 °C the A/(A + B) ratio is about 0.9 and the B/(A + B) ratio is 0.1 (Fig. 4). The B/(A + B) ratio decreases with increasing temperature. However, for a given temperature, this ratio remains constant with increasing time (1 to 30 days; Table 4; Fig. 4).

Selected area diffraction and HRTEM observations

SAD patterns of the unheated monazite (Fig. 5a) always show sharp reflections. No differences between these SAD patterns and the SAD patterns of the sample heated at 900 °C were observed. However, HRTEM image of the unheated monazite revealed isolated areas (5 nm^2) where the lattice fringes were blurred or absent (Fig. 5a). The distorted areas pose strain on the lattice in the vicinity, which causes inhomogeneous contrast distribution close to the distorted areas (Fig. 5a). These

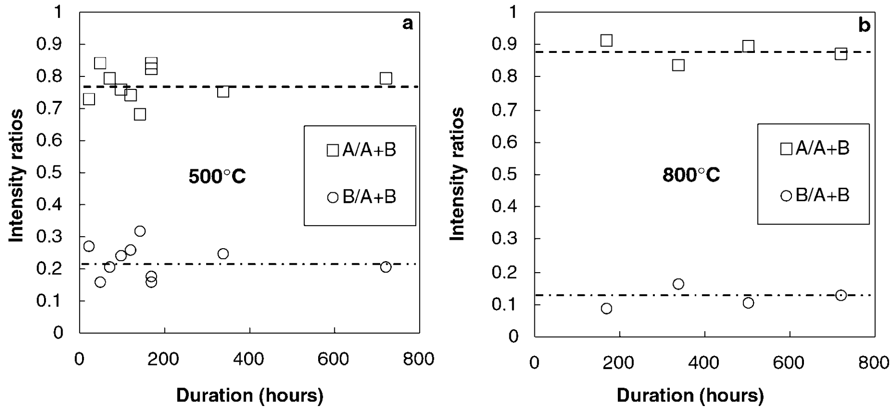

Fig. 4a, b Evolution of the amplitude ratios of the two phases *A* and *B* as a function of time. **a** At 500 °C. **b** At 800 °C. *A* corresponds to the sharp reflections and *B* to the broad reflections

Table 4 Amplitude ratios of the (200) reflections of the two phases *A* and *B* at 500 and 800 °C as a function of time

Durations (h)	500 °C			800 °C		
	Experiment no.	A/(A + B)	B/(A + B)	Experiment no.	A/(A + B)	B/(A + B)
24	Mo500-24	0.73	0.27	–	–	–
48	Mo500-48	0.84	0.16	–	–	–
72	Mo500-72	0.80	0.20	–	–	–
96	Mo500-96	0.76	0.24	–	–	–
120	Mo500120	0.74	0.26	–	–	–
144	Mo500-6d	0.68	0.32	–	–	–
168	Mo500-7d	0.82	0.18	Mo800-7d	0.91	0.09
336	Mo50014d	0.75	0.25	Mo80014d	0.84	0.16
504	–	–	–	Mo80021d	0.90	0.10
720	Mo50030d	0.79	0.21	Mo80030d	0.87	0.13

distorted domains completely disappeared at 900 °C: HRTEM images of this monazite showed undistorted lattice fringes and homogeneous contrast (Fig. 5b).

Dark field images

Dark-field (DF) images of the unheated monazite (Fig. 6a) show mottled diffraction contrast as a result of a mosaic structure of the crystal. The slightly differently oriented domains, which represent coherent scattering volumes with slightly varying orientations, are quite homogeneously distributed in the monazite. The bright areas, e.g. Fig. 6a, represent small coherent scattering volumes, which have no or only a small deviation from the exact Bragg position. At 500 °C these domains were still observed. However, the coherent scattering volumes became larger (Fig. 6b). At 800 °C, only small amounts of the distorted domains remained (Fig. 6c) and they are no longer observed at 900 °C (Fig. 6d).

Line scans across different volumes of monazite showed no detectable change in its chemical composition, thus indicating the chemical homogeneity of this monazite.

Raman measurements

The Raman spectra of monazites annealed at high temperature (Fig. 7) show distinctly narrower bands than the reference spectrum of the untreated monazite, which generally displays only moderate band broadening.

Monazite annealed at 500 °C shows only moderately decreased Raman band broadening. Raman spectral parameters obtained from samples annealed between 800 and 1200 °C are identical within their errors (Table 5). This implies that at 800 °C, the recovery of the short-range order was almost as complete as after annealing at 1200 °C.

Cathodoluminescence

The CL results are only briefly documented here and will be described in more detail elsewhere. CL images of monazites were taken from areas $30 \times 120\ \mu m^2$ in size. Four sample images are presented in Fig. 8. We did not observe notable inhomogeneities, which confirms the above statement that the studied monazite is chemically homogeneous at a microscale. Series of images were obtained in order to check potential changes of the relative CL signal intensity with annealing. In Fig. 8 it can be seen that annealed monazites emit more intense CL than the untreated sample. Corresponding with the other analytical results, most changes are observed between 500 and 800 °C, whereas above 800 °C intensity variations are insignificant.

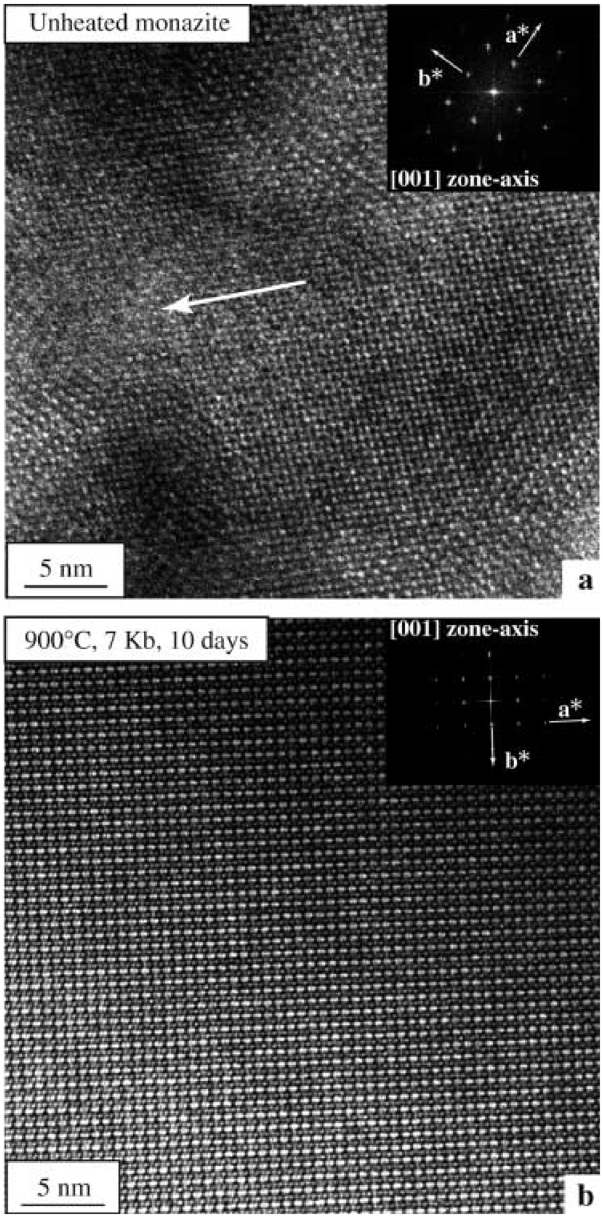

Fig. 5 a Energy-filtered HRTEM image and corresponding diffraction pattern (fast Fourier transform) of the unheated monazite. Note the presence of distorted domains (*arrow*). **b** Energy-filtered HRTEM image and corresponding diffraction pattern (FFT) of the monazite heated at 900 °C, 7 Kb, 10 days (VRM98-1). The lattice fringes are not distorted

Discussion

Interpretation of the results

X-ray diffraction patterns of the unheated monazite show the coexistence of two diffraction domains A and B, which can be interpreted as two monazite phases with slightly different lattice parameters and different crystallinity (Table 3). The first one, A, shows sharp reflections of high amplitudes (Fig. 2b) indicating that A corresponds to a well-ordered, well-crystallised monazite with larger unit-cell volume (302.60 Å^3). The second domains, B, show broad reflections of low amplitudes, 3.5 times lower than A (Table 3). Diffraction domains B are interpreted as a distorted monazite crystal lattice composed of islands with an expanded lattice, induced by presence of interstitials, and islands of a compressed monazite lattice, induced by presence of vacancies. These vacancies and interstitials (Frenkel pairs) are the result of α-recoil damage (Fig. 9a,b). The recoiled heavy nucleus knocks atoms from the lattice position into an interstitial position. The interstitials induce an expansion of the unit-cell volume of adjacent crystalline areas. The removed atoms create vacancies causing slight relaxations of the lattice (Fig. 9b). The islands of both expanded and contracted lattice will pose stress on the lattice vicinity, which is visible in the HRTEM images (Fig. 5a) and accounts for the decreased short-range order causing Raman band broadening. The broadening (XRD) of the B reflection, with its centre at the position of the reference reflection (Ni et al. 1995), is due to the expanded or compressed diffraction domains and additional small particle size. Furthermore, expansion of the A domains will also exert stress on the B domains. The similar area percentages of the two domains show that the volume fraction of A in monazite seems to be the same as for B. Possible reasons for the expansion of the A-monazite lattice are discussed below.

Concerning the kinetics, we conclude that after 24 h and even at 800 °C the annealing process is too slow to cause a significant change of the A/B amplitude ratios (Fig. 4, Table 4) within experimental conditions (here 30 days). This is in agreement with the generally slow rate of cation diffusion in monazite (Suzuki et al. 1994; Smith and Giletti 1997; Montel and Seydoux 1998). We suggest that during the 24 first hours, He diffuses faster out of the crystal due to the radiation damage in domains B. At the same time there is a rearrangement of the atoms by diffusion in these domains. This diffusion will be relatively fast if the vacancies and the interstitials are not so far from each other. However, there is a moment where the atoms are too far away and where the diffusion will be too slow (after 20 hours). This might explain why the A/(A + B) or B/(A + B) ratios are quite constant (Fig. 4). Thus, He diffusion becomes too slow and He is trapped in the monazite lattice.

The TEM results (HRTEM and DF) support also the presence of two domains: nm-sized domains with blurred lattice fringes and well-crystallised domains (Fig. 5a). According to the XRD results, we refer the A phase to these crystallised domains and the B phase to the distorted nm-sized domains. Consequently, the unheated monazite is a mosaic crystal composed of well-crystallised domains A and nm-sized distorted regions B.

With increasing annealing temperature, XRD patterns of the monazite exhibit lower amplitude of the broad reflections B (Fig. 3, Table 3). This is also supported by TEM images (DF) with a gradual coarsening of the mosaic structure (Fig. 6b,c). We interpret this as a

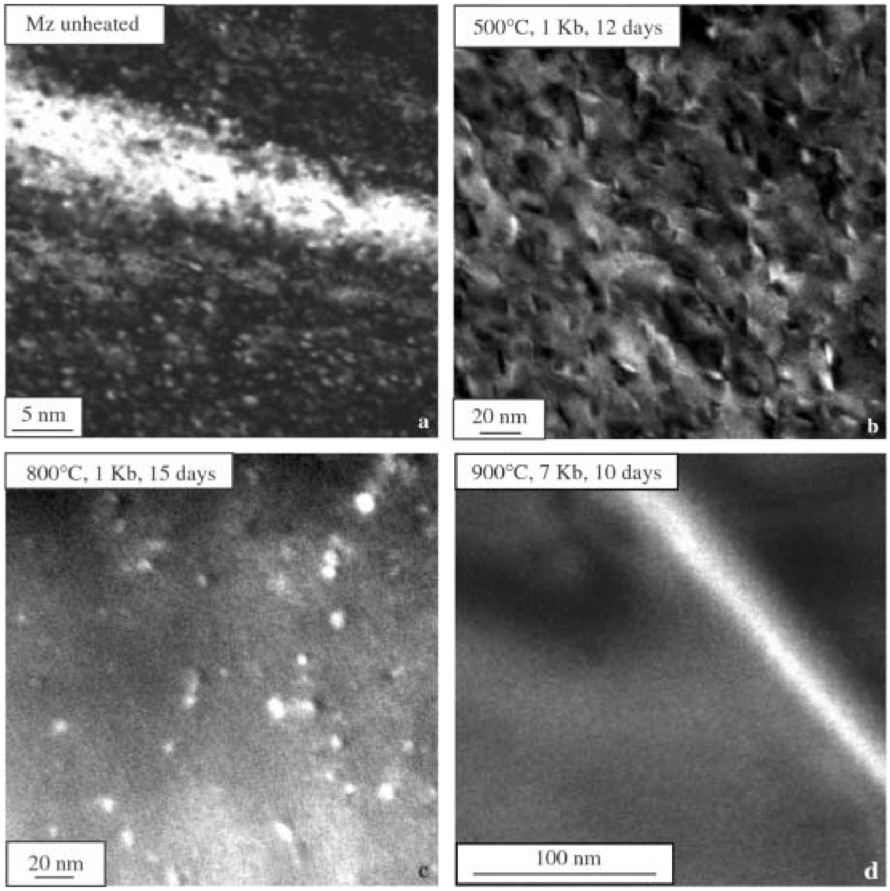

Fig. 6a–d TEM dark-field images (DF). **a** Unheated monazite. Mottled diffraction contrast is due to the presence of distorted areas. Their distribution is quite homogeneous in the grain. **b** Monazite heated at 500 °C, 1 Kb, 12 days (VRM97-1). Mottled diffraction contrasts are still present. However the coherent scattering volumes became larger. **c** Monazite heated at 800 °C, 1 Kb, 15 days (VRM97-2). Only a small amount of the distorted domains remained. **d** Monazite heated at 900 °C, 7 Kb, 10 days (VRM98-1). No more distorted areas are visible

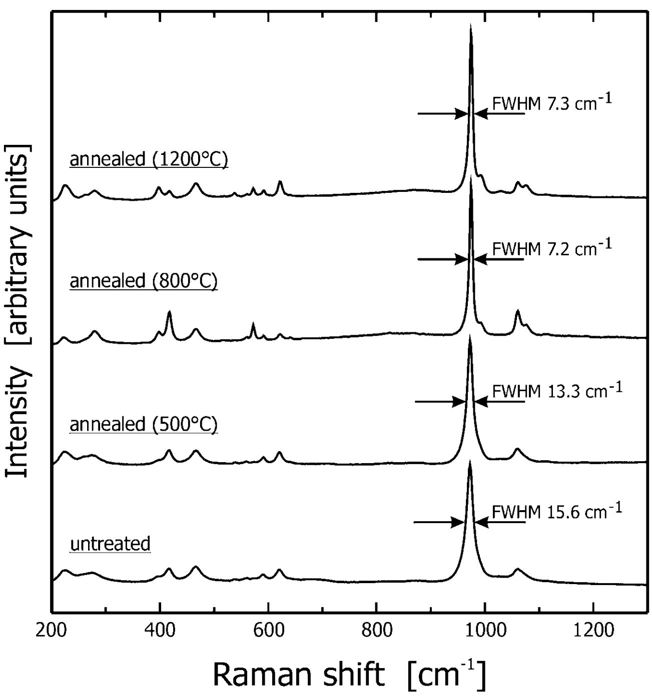

Fig. 7 Raman spectra of the untreated monazite in comparison with spectra of annealed samples. Note the decreasing width of the $\nu_1(PO_4)$ band (the intense peak at ≈972–974 cm^{-1}). Measured FWHMs are given

progressive healing of defects in distorted domains B with increasing temperature. On the contrary, the FWHM of A reflections remain unchanged and minimum (~0.09°) with increasing temperature, suggesting that the A domains in the unheated monazite were already well crystallised (Table 3). The complete absence of the broad reflections in the XRD pattern at 1000 °C correlates with the absence of the distorted domains in the HRTEM image (Fig. 5b) and a homogeneous diffraction contrast on the DF image (Fig. 6d). At 900 °C the presence of a well-crystallised monazite lattice indicates complete healing of the structural radiation damage.

Raman spectroscopy was introduced by Nasdala et al. (1995) as a method to estimate the degree of metamictization. These authors found that the gradually decreasing short-range order in metamict zircons causes increasing broadening of Raman bands, accompanied by frequency shifts towards lower wavenumbers due to the general widening of bond lengths. However, in the case of monazite, decreased short-range order, together with Raman band broadening and shifted peak positions, is not necessarily due to radiation damage but may also be caused by deviations from the ideal chemical composition. For example, internal PO_4 vibrations become irregular when the next neighbouring Ce^{3+} ions are partially replaced by other ions such as Th^{4+}, Ca^{2+}

Table 5 Spectral parameters of the $\nu_1(PO_4)$ Raman band

Sample	Annealing temperature (°C)	Annealing pressure (kbar)	Bandposition (cm^{-1})	Measured FWHM (cm^{-1})	Corrected FWHM[a] (cm^{-1})
Untreated	–	–	972.2	15.6 ± 1.0	15.0 ± 1.0
VRM97-1	500	1	972.5	13.3 ± 1.0	12.6 ± 1.0
VRM97-2	800	2	974.3	7.2 ± 0.7	5.8 ± 0.7
VRM97-4	900	1	974.4	7.1 ± 0.7	5.7 ± 0.7
VRM98-1	900	7	974.3	7.4 ± 0.7	6.1 ± 0.7
VRM97-10	1000	7	974.4	7.3 ± 0.7	5.9 ± 0.7
VRM97-8	1100	7	974.4	7.3 ± 0.7	5.9 ± 0.7
VRM97-6	1200	7	974.4	7.3 ± 0.7	5.9 ± 0.7

[a] Measured FWHMs were corrected for the apparatus function (here 3 cm^{-1}) and real FWHMs were calculated according to Irmer (1985)

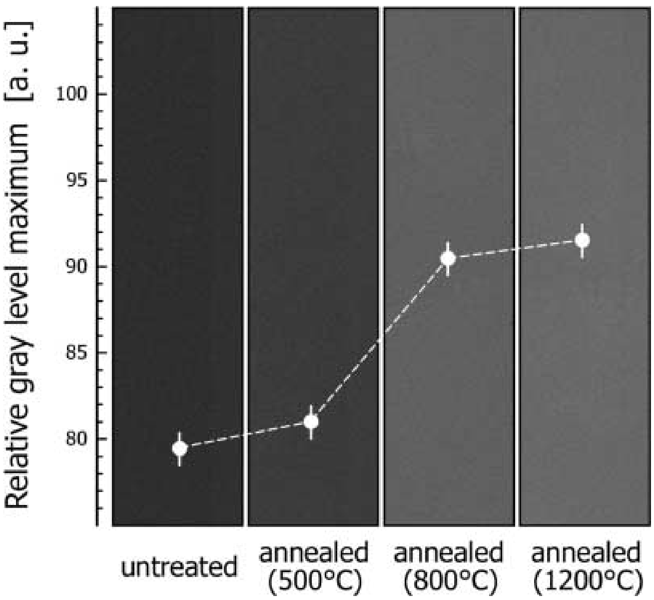

Fig. 8 CL images of the same four samples as in Fig. 7. The relative intensity of the area-integrated CL signal was measured on a random greyscale (0 = *black*; 256 = *white*). The *values at the ordinate axis* represent the maxima of the respective greyscale distribution patterns

or other REEs. Correspondingly, Podor (1995) demonstrated that Raman spectra of synthetic REE phosphates show systematic band broadening and peak shifts with increasing actinide content. Nasdala et al. (1999) obtained significantly broadened Raman spectra from natural monazites that were well crystalline, in spite of a Th content exceeding 10 wt% and a self-irradiation dose exceeding 5×10^{16} α/mg. Taking into account that the Raman spectrum might be structurally and chemically affected, a quantitative estimation of the degree of radiation damage in monazite from the Raman spectra only is limited. However, it is possible to analyse the spectra obtained from our chemically identical samples in view of potentially different contributions of their different degrees of radiation damage to the Raman spectral parameters. Observations in Fig. 7 suggest that a major portion of the initial Raman band broadening is caused by radiation damage. The greatly enhanced short-range order of the heat-treated samples points to structural recovery during annealing. This is also consistent with the observed moderate band shifts towards higher wavenumbers (Table 5). Our observations suggest that most of the healing of the initially metamict structure must have occurred between 500 and 800 °C.

Although quantitative conclusions are limited at the present stage, the comparison of the obtained spectra (Fig. 7) with the Raman band broadening of other radiation-damaged minerals such as zircon (Nasdala et al. 1995) and biotite (Nasdala et al. 2001a) suggests that the untreated monazite sample must be moderately metamict. The observed $\nu_1(PO_4)$ band broadening (structurally caused FWHM increase ~ 9 cm^{-1}) indicates significant radiation damage. On the other hand, the Raman spectrum of the untreated sample is dominated by Raman bands of disordered but still crystalline monazite whereas the spectrum of the amorphous phase is insignificant (Nasdala et al. 2001b). This is consistent with the TEM observations presented above.

The CL results confirm first that monazites are comparably poor CL emitters: the recorded CL intensity was generally low and high signal amplification was needed to produce greyscale images. The significantly enhanced CL intensity after annealing suggests that the CL emission of monazite is not only determined by the chemical composition as, for example the content of 4*f* elements (REE). Recall that the CL images shown in Fig. 8 were obtained from samples with identical chemical composition. These observations give strong evidence that the CL emission depends notably on structural features such as the short-range order, which was in our case controlled by radiation damage (L. Nasdala et al. accepted in Chem. Geol.). According to the observed degree of CL recovery upon annealing, most structural reconstitution must have occurred between 500 and 800 °C, which is consistent with the XRD and Raman results.

The problem of the A-monazite lattice expansion

In the following we try to explain the lattice expansion, which is observed in the A domains (crystalline domains), and what happens during increasing annealing temperature. Two different hypotheses are proposed.

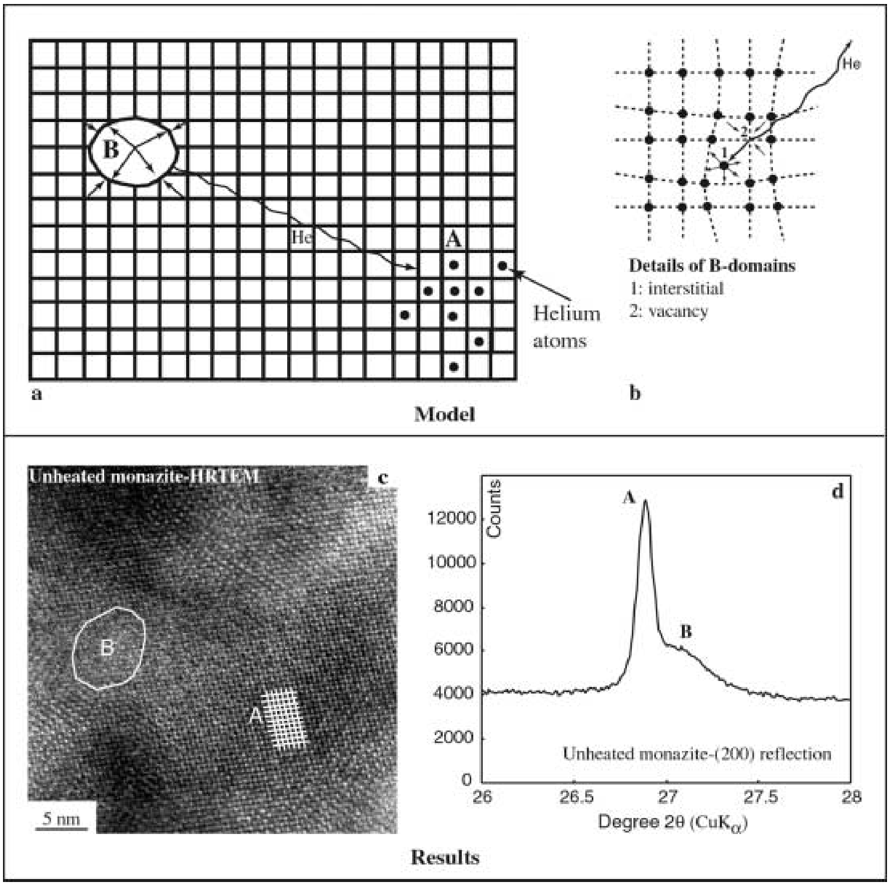

Fig. 9a–d Model describing the *A* and *B* domains (**a** and **b**). The results from HRTEM and XRD from the unheated monazite are given in **c** and **d**. During an alpha event a heavy atom nucleus liberates its energy by ejecting an alpha particle. The remaining nucleus recoils in an opposite direction from the alpha particle. This recoil creates Frenkel pairs, i.e. interstitial atom *1* and vacancy *2*, which exert stress on the lattice in the vicinity (see **b**). These distorted domains correspond to the domains B. They are interpreted as a helium-free distorted monazite crystal lattice, which can be referred to old alpha-recoil tracks, and is composed of islands with an expanded lattice, induced by presence of interstitials (*1*), and islands of a compressed monazite lattice, induced by presence of vacancies (*2*). Both the islands will pose stress on the lattice in the vicinity (see **b**). The broadening of the B reflection in **d** is due to the expanded or compressed diffraction domains and the different amount of distortion. Helium accumulates in the crystalline regions *A* (see **a** and **c**) and induces an expansion of the unit-cell volume (see **d**). During the heating, domains B are healed, then progressively disappear. Helium diffuses out of the monazite lattice, inducing a relaxation of the lattice of the regions A. At 900 °C, healing of the lattice is completed

Presence of Frenkel defects

We interpret the distorted B domains as old alpha-recoil tracks. These isolated islands are expanded or can be compressed, and consequently compress or expand the adjacent crystalline regions of the sample (Lumpkin and Ewing 1988; Salje et al. 1999). Expansion of A results in compressive stress on B. However, the A unheated monazite (Moacir 0) shows a well-crystallised lattice with a volume increase of 1% compared with monazite, which was annealed at 1000 °C (Table 3). The expansion has been explained previously with the presence of Frenkel defects (Murakami et al. 1986, 1991; Weber et al. 1998). As demonstrated by Nasdala et al. (2001a), such point defects cannot be resolved by HRTEM and XRD.

With increasing temperature, Frenkel defects are healed, i.e. interstitial cations diffuse into the vacant sites, resulting in a relaxation of the lattice and a shift of the A reflections to smaller d_{hkl} values. Alpha-recoil tracks are healed and consequently the B domains disappear.

This hypothesis is not in full agreement with our observations. For example, we do not observe in XRD a reduction of the peak width due to ordering of interstitial atoms with increasing temperature. Furthermore, interstitials in the A lattice will induce an expansion of the lattice, which can be compensated for by the relaxation induced by vacancies. This would be in contradiction to the observed increase of the lattice parameters.

Presence of helium

Using the measured U, Th contents, we calculated that the studied monazite has experienced about 2.43×10^{16} alpha-decay events/mg since its growth 474 Ma ago. We have calculated that each gram of the monazite produced 0.17 mg of helium. Measurements of the He content on aliquots of the Moacir monazite are in agreement with the calculated content, and lead to U/Th–He age of 479 Ma (R. Pik 2001, personal communication). This age is concordant with the U/Pb age, indicating that all the helium accumulated in the crystal's lifetime has been stored in the monazite lattice. Such a large amount of helium should expand the monazite lattice (Weber et al. 1998).

It seems to be unlikely that He is accumulated in domains corresponding to the broad B reflections, as the crystal lattice is distorted in these domains (Fig. 9b,c), unable to trap atoms. The sharp reflections A correspond to the well-crystallised areas where helium atoms are homogeneously distributed, thus inducing an expansion of the monazite lattice. Homogeneously distributed helium in these domains will not modify the periodicity of the unit cell, i.e. the FWHM of monazite [$=0.09°(2\theta)$], which is in agreement with our results.

During heating, the alpha-recoil tracks are healed, then disappear progressively. Simultaneously with the healing of the alpha-recoil tracks with annealing, helium diffuses out of the monazite lattice, inducing a relaxation of the lattice. This results in a decrease of the unit-cell volume, i.e. A reflections shift to higher 2θ values (smaller d_{hkl} values) but the FWHM of A remains constant. Erichsen (1951) demonstrated that at 600 °C only about 50% of the total He of the monazite is lost. This is in agreement with our XRD results, which still showed an expansion of domains A at 500 °C.

A rough estimate of the accumulated He in monazite can be made using a very simple solid sphere model: 2.5×10^{16} He/mg is about 0.01 mol He in 1 mol of monazite. The volume occupied by atoms in 1 mol of monazite, calculated from the composition given in Table 1, is 30.71 cm^3. The volume of 0.01 mol of He atoms (atomic radius 1.28 Å) is then 0.053 cm^3. Hence, the increase in volume due to the presence of He is about 0.2%. The observed relative variation in volume change of the unit cell during the annealing process is 1%, five times more than calculated. The discrepancy is not large considering two arguments. First, in this model, all the He atoms are assumed to be accumulated only in the volume fraction represented by the sharp reflections A. Consequently, the amount of He in the undistorted lattice volume A is larger than if distributed in all the monazite, i.e. in A plus B domains. Second, the method we used to estimate the effect of He on the monazite structure is very crude because it takes into account only volumes, and not geometry. Therefore, we conclude that as far as volume is concerned, the He accumulation may explain the order of magnitude of expansion observed in undistorted regions A.

Comparison with previous studies

In the Introduction, we mentioned some contradictions in the literature concerning the annealing temperature of monazite. Two different temperature ranges are proposed: between 300 (Karioris et al. 1981; XRD study) and 450 °C (Meldrum et al. 1998; HRTEM study) and between 1100 °C (Smith and Giletti 1997; XRD study) and 900 °C (this study). The first difference, between 300 and 450 °C, is attributed to the fact that XRD methods are not sensitive enough to exactly determine if a structure is completely healed or still contains some defects (cf. this study). The difference between our study and that of Smith and Giletti (1997) is explained by the same argument.

Considering the difference between 450 °C (Meldrum et al. 1998) and 900 °C (this study) we would argue that the starting material was different for these studies. A completely metamict monazite, amorphized by 800 KeV Kr^+ ions, was used by Meldrum et al. (1998), while our starting material was a crystalline monazite with a small amount of defects. The differences in temperature may be due to the type of healing process: epitaxial recrystallisation vs. diffusion. Epitaxial recrystallisation starts immediately after the beginning of nucleation (not observed in our study). We observed that the diffusion rate is very slow and healing of defects by diffusion needs higher temperature to be more efficient. Metamict monazite begins to recrystallise at about 450 °C. The lattice defects of crystalline monazite, which contains isolated distorted domains due to irradiation damage, are healed at about 900 °C. This observation concurs very well with recent results of Nasdala et al. (2001b), who found that isolated Frenkel pairs are a comparably stable type of radiation damage, whereas more radiation-damaged clusters are more easily annealed.

Furthermore, it is important to note that these studies treat annealing without considering the competing amorphisation process. In nature, there is always competition between these two processes. Many studies illustrate that monazite already healed at 200 °C (Meldrum et al. 1996, 1997, 1998, 1999, 2000).

Differences between monazite and zircon

The reflection broadening in XRD patterns mentioned above was already observed in the monazite used by Smith and Giletti (1997). However, the resolution of their diffractometer was not sufficient to clearly separate the two reflections, and therefore, the authors did not interpret the diffraction pattern. Nevertheless, it is obvious that the raw monazite (200) reflection is composed of two reflections: a sharp one on the left and a broad one on the right. The broad reflection decreases with increasing temperature and totally disappears at the annealing at 1100 °C, just as in our study.

Murakami et al. (1991) investigated irradiation damage in a suite of natural zircon samples that span a range of doses over which the transition from the crystalline to amorphous metamict state occurred. They defined three different stages of damage accumulation. Our starting monazite is equivalent to Murakami's Ib stage, which corresponds to a crystalline monazite with nm-sized distorted domains. Murakami et al. (1986, 1991) described the XRD (200) pattern of zircon in stage Ib as an asymmetric reflection resulting from a combination of a Bragg diffraction maximum and a diffuse scattering component. We supposed that this asymmetry is visible only because they used a low-resolution diffractometer. The Bragg diffraction component may correspond to the reflection A in our study and the diffuse scattering component may be referred to the reflection B. The authors report that the symmetric Bragg diffraction maximum shifts to smaller values of 2θ with increasing dose (increasing unit-cell volume), which is in agreement with our observations. The diffuse scattering component in the diffraction pattern is assigned to interstitial defects. This explanation seems not to be appropriate, because the presence of defects should increase the lattice volume, i.e. a diffuse scattering component should be located at smaller scattering angles. We suggest explaining the diffuse scattering component in terms of the reflection B observed in our study.

Applications for geochronology

Considering that minerals are fully amorphized after accumulating about 0.3–0.5 dpa (e.g. Weber et al. 1994), the studied monazite with a self-irradiation dose of about 2 dpa cannot have accumulated the complete radiation damage since the time of its growth 474 Ma ago. In contrast, only a small portion of the damage is stored, whereas most of the radiation damage must have been healed. However, the healing of the radiation damage has not affected the U–Th–Pb isotope system of the monazite, which still yields concordant ages.

Pb diffusion in monazite is assumed to be very slow (Suzuki et al. 1994; Smith and Giletti 1997). However, radiation damage can increase the rate of diffusion, because these defects provide channels for the diffusion. Resetting of monazite depends on the behaviour of its crystal lattice with temperature. If the monazite lattice is destroyed by irradiation, Pb can be lost by diffusion through these channels, i.e. interface between crystalline and amorphous domains. If the monazite lattice is pristine, Pb diffusion will not be an efficient mechanism for resetting, because of the slow rate of Pb diffusion in monazite; resetting occurs by a dissolution–precipitation process.

As already said, it is generally observed in nature that monazite is very often crystalline, because irradiation damage is rapidly healed at low temperature. This means that, in geologic samples, Pb diffusion occurs predominantly within a pristine, organised crystal structure. To conclude, discordant U–Pb ages obtained for monazite mainly result from resetting by dissolution–precipitation.

Cherniak (1993) studied the Pb diffusion in titanite. She demonstrated that metamict titanite is much less retentive for Pb, and that Pb isotope ratios should rarely be preserved in this structure. The author calculated the closure temperatures, i.e. the temperature at which the daughter nuclide begins to accumulate in the structure, for metamict and crystalline titanite. A titanite crystal (0.005-cm diameter) will still retain Pb isotope information when heated at 600 °C for several million years. In contrast, a metamict titanite of the same size will retain Pb only when heated at a temperature < 200 °C, for several million years. Furthermore, Zhang and Schärer (1996) found a magmatic titanite, which contains an inherited radiogenic Pb component. This means that titanite was not totally reset during magmatic new growth at temperature higher than 712 °C. All these results show that closure temperature for minerals should be used carefully. We cannot explain an age discordance by simply using the closure temperature of a mineral, because it depends also greatly on the lattice of the mineral, metamict or crystalline. This might explain the reported differences in closure temperature of monazite between 720 and 750 °C (Copeland et al. 1988) and 530 ± 25 °C (Black et al. 1984).

Implications for nuclear waste

Monazite is studied in order to check its ability to incorporate large amounts of actinides and to investigate its resistance to dissolution and irradiation damage. The aim is to find crystalline ceramics with a monazite-like structure as a container for high-level nuclear waste (Boatner et al. 1980, 1981; Boatner and Sales 1988).

Our study shows that although old (474 Ma), rich in U and Th (1300 ppm of U and 69 000 ppm of Th), and containing small irradiation damages at the nanometer scale, our monazite is not metamict, because of its ability to repair damage domains at relatively low temperature. Irradiation experiments show that monazite cannot be amorphized at temperatures exceeding 200 °C (Meldrum et al. 1997, 1998). This means that radiation damages cannot accumulate in monazite because during annealing the defects are healed faster than the lattice is damaged. Therefore, it can be speculated that nuclear waste in a monazite-ceramic will remain in a crystalline state nearly forever.

Conclusions

It is concluded that the investigated Brazilian monazite is like a mosaic crystal. The mosaic consists of two domains A and B, which are basically two monazite crystals with slightly different lattice parameters. Diffraction domains A show sharp reflections with high amplitude. They are assigned to a well-crystallised lattice with small volume expansion (1%). Diffraction domains B exhibit very broad reflections with low amplitude and represent a distorted lattice, which can be referred to old alpha-recoil tracks. We calculated that about 2.5×10^{16} α/mg have been accumulated in this monazite since its formation, 474 Ma ago. It is suggested that the A domains correspond to well-crystallised areas where helium atoms are trapped. The trapped He causes an expansion of the monazite lattice A. Consequently, the A reflections are shifted to smaller scattering angles 2θ. Diffraction domains B are interpreted as a distorted monazite crystal lattice composed of islands with an expanded lattice (interstitials), and islands of a compressed monazite lattice, (vacancies). Both the islands will pose stress (compression and/or dilatation) on the lattice in the vicinity. The broadening of the B reflections is due to the expanded/compressed diffraction domains and due to the different amount of the distortion. Therefore, in the B domains, helium cannot accumulate because the crystal net is very poor, unable to trap atoms.

During annealing, the alpha-recoil tracks are healed, and the diffraction domains B progressively disappear. At the same time, helium diffuses out of the monazite lattice, inducing a relaxation of the lattice (volume decrease). The A reflections are shifted to larger scattering angles (smaller d_{hkl} values). At 900 °C only one phase remains, that is a monazite with well-crystallised lattice and minimum unit-cell volume.

Why is monazite never metamict? Although it is obvious that monazite is able to heal its structure at low temperature (100–200 °C), it is not certain that this low temperature annealing is the only effect. It is surprising that during annealing nearly all the helium remains accumulated in the monazite lattice. It is also possible to consider an ionisation-annealing induced by helium-ion irradiation, a phenomenon observed in apatite (Ouchani et al. 1997). This is in agreement with the assumption that the well-crystallised domains correspond to the helium-rich domains.

Acknowledgements We would like to thank very much Moacyr Marinho (UFBA, Brazil), who kindly provided us with the monazite sample. We thank I. Bauer (GFZ) for providing the XRD analyses and E.M. Schemmert and K. Paech (GFZ) for the preparation of the TEM samples. We are grateful to A. Kronz (University of Göttingen) for taking the CL images. A. Beran and E. Libowitzky (University of vienna) kindly made a Raman system available for analysis. Thanks to R. Pik (CRPG-Nancy, France) for his personal communication concerning the U/Th–He age of our monazite. Official reviews by A. Deutsch and an anonymous reviewer considerably improved the quality of this paper.

References

Black LP, Fitzgerald JD, Harley SL (1984) Pb isotopic composition, colour, and microstructure of monazites from a polymetamorphic rock in Antarctica. Contrib Mineral Petrol 85: 141–148

Boatner LA, Sales BC (1988) Monazite. In: Lutze W, Ewing RC (eds Radioactive waste forms for the future. Elsevier, New York, pp 495–564

Boatner LA, Beall GW, Abraham MM, Finch CB, Huray PG, Rappaz M (1980) Monazite and other lanthanide orthophosphates as alternative actinide waste forms. In: Northrup CJM Jr (ed) Scientific basis for nuclear waste management 2. Plenum Press, New York, pp 289–296

Boatner LA, Abraham MM, Rappaz M (1981) The characterization of nuclear waste forms by EPR spectroscopy. In: Moore JG (ed) Scientific basis for nuclear waste management 3. Plenum Press, New York, pp 181–188

Cherniak DJ, Lanford WA, Ryerson FJ (1991) Lead diffusion in apatite and zircon using ion implantation and Rutherford backscattering techniques. Geochim Cosmochim Acta 55: 1663–1673

Cherniak DJ (1993) Lead diffusion in titanite and preliminary results on the effect of radiation damage on Pb transport. Chem Geol 110: 177–194

Cocherie A, Legendre O, Peucat JJ, Kouamelan AN (1998) Geochronology of polygenetic monazites constrained by in situ electron microprobe Th–U-total lead determination: implications for lead behaviour in monazite. Geochim Cosmochim Acta 62: 2475–2497

Copeland P, Parrish RR, Harrison TM (1988) Identification of inherited radiogenic Pb in monazite and its implications for U–Pb systematics. Nature 333: 760–763

Corfu F (1988) Differential response of U–Pb systems in coexisting accessory minerals, Winnipeg River Subprovince, Canadian Shield: implications for Archean crustal growth and stabilization. Contrib Mineral Petrol 98: 312–325

Cruz MJ, Cunha JC, Merlet C, Sabaté P (1996) Datação pontual das monazitas da região de Itambé, Bahia, através da microssonda electrônica. XXXIX Congresso Brasileiro de Geologia

Dodson MH (1973) Closure temperature in cooling geochronological and petrological systems. Contrib Mineral Petrol 40: 257–259

Erichsen LV (1951) Über die Heliumabgabe von Monazit in Abhängigkeit von Gasphase, Druck und Temperatur. N Jb Mineral. Monatshefte: 25–33

Ewing RC (1975) The crystal chemistry of complex niobium and tantalum oxides IV. The metamict state: discussion. Am Mineral 60: 728–733

Ewing RC, Chakoumakos BC, Lumpkin GR, Murakami T, Gregor RB, Lytle FW (1988) Metamict minerals: natural analogues for radiation damage effects in ceramic nuclear waste forms. Nucl Instr Meth(B)32: 487–497

Ewing RC, Weber WJ, Clinard FW Jr (1995) Radiation effects in nuclear waste forms. Progr Nucl Energy 29: 63–127

Ewing RC, Meldrum A, Wang LM, Wang SX (2000) Radiation-induced amorphization. In: Ribbe PH (ed) Reviews in mineralogy and geochemistry, vol 39. Mineralogical Society of America, Washington DC, pp 319–361

Förster HJ (1998) The chemical composition of REE–Y–Th–U-rich accessory minerals in peraluminous granites of the Erzgebirge-Fichtelgebirge region, Germany, Part I: The monazite-(Ce)-brabandite solid solution series. Am Mineral 83: 259–272

Gögen K, Wagner GA (2000) Alpha-recoil track dating of Quaternary volcanics. Chem Geol 166: 127–137

Irmer G (1985) Zum Einfluß der Apparatefunktion auf die Bestimmung von Streuquerschnitten und Lebensdauern aus optischen Phononenspektren. Exper Techn Phys 33: 501–506

Karioris FG, Appaji Gowda K, Cartz L (1981) Heavy ion bombardment of monoclinic $ThSiO_4$, ThO_2 and monazite. Rad Eff Lett 58: 1–3

Krohe A, Wawrzenitz N (2000) Domainal variations of U–Pb monazite ages and Rb–Sr whole-rock dates in polymetamorphic paragneisses (KTB Drill Core, Germany): influence of strain and deformation mechanisms on isotope systems. J Metamorph Geol 18: 271–291

Landzirotti A, Hanson GN (1995) U–Pb dating of major and accessory minerals formed during metamorphism and deformation of metapelites. Geochim Cosmochim Acta 59: 2513–2526

Larson AC, Von Dreele RB (1988) GSAS-generalized structure analysis system. Los Alamos Nat Lab Rep LAUR, 86–758, 1–150

Lumpkin GL, Ewing RC (1988) Alpha-decay damage in minerals of the pyrochlore groups. Phys Chem Miner 16: 2–20

Meldrum A, Wang LM, Ewing RC (1996) Ion-beam-induced amorphization of monazite. Nucl Instr Meth Phys Res (B) 116: 220–224

Meldrum A, Boatner LA, Ewing RC (1997) Electron-irradiation-induced nucleation and growth in amorphous $LaPO_4$, $ScPO_4$, and zircon. J Mat Res 12: 1816–1827

Meldrum A, Boatner LA, Weber WJ, Ewing RC (1998) Radiation damage in zircon and monazite. Geochim Cosmochim Acta 62: 2509–2520

Meldrum A, Boatner LA, Zinkle SJ, Wang SX, Wang LM, Ewing RC (1999) Effects of dose rate and temperature on the crystalline-to-metamict transformation in the ABO_4 orthosilicates. Can Mineral 37: 207–221

Meldrum A, Boatner LA, Ewing RC (2000) A comparison of radiation effects in crystalline ABO_4-type phosphates and silicates. Mineral Mag 64: 183–192

Montel JM, Seydoux AM (1998) Sm–Nd interdiffusion in monazite. EMPG VII, Terra Nova 10, Abstr. Supl: 42

Murakami T, Chakoumakos BC, Ewing RC (1986) X-ray powder diffraction analysis of alpha-event radiation damage in zircon ($ZrSiO_4$). In: Clark DE, White WB, Machiels J (eds) Advances in ceramics: nuclear waste management II. Am Cer Soc, Columbus, Ohio, 20: 745–753

Murakami T, Chakoumakos BC, Ewing RC, Lumpkin GR, Weber WJ (1991) Alpha-decay event damage in zircon. Am Mineral 76: 1510–1532

Nasdala L, Massonne H-J (2000) Microdiamonds from the Saxonian Erzgebirge, Germany: in situ micro-Raman characterisation. Eur J Mineral 12: 495–498

Nasdala L, Wolf D, Irmer G (1995) The degree of metamictization in zircon: a Raman spectroscopic study. Eur J Mineral 7: 471–478

Nasdala L, Pidgeon RT, Wolf D (1996) Heterogeneous metamictization of zircon on a microscale. Geochim Cosmochim Acta 60: 1091–1097

Nasdala L, Finger F, Kinny P (1999) Can monazite become metamict? Eur J Mineral 11, Beih 1: 164

Nasdala L, Wenzel M, Andrut M, Wirth R, Blaum P (2001a) The nature of radiohaloes in biotite. Am Mineral 86: 498–512

Nasdala L, Wenzel M, Vavra G, Irmer G, Wenzel T, Kober B (2001b) Metamictisation of natural zircon: Accumulation versus thermal annealing of radioactivity-induced damage. Contrib Mineral Petrol 141: 125–144

Nasdala L, Lengauer CL, Hanchar JM, Kronz A, Blanc P, Kennedy AK, Seydoux-Guillaume AM. Annealing metamictization and the recovery of cathodoluminescence. Submitted in Chem Geol

Ni Y, Hughes JM, Mariano AN (1995) Crystal chemistry of the monazite and xenotime structures. Am Mineral 80: 21–26

Ouchani S, Dran JC, Chaumont J (1997) Evidence of ionization annealing upon helium-ion irradiation of pre-damaged fluorapatite. Nucl Instr Meth Phys Res B132: 447–451

Owen MR (1988) Radiation-damage halos in quartz. Geology 16: 529–532

Paquette JL, Montel JM, Chopin C (1999) U–Th–Pb dating of the Brossasco ultrahigh-pressure metagranite, Dora-Maira massif, western Alps. Eur J Mineral 11: 69–77

Parrish RR (1990) U–Pb dating of monazite and its application to geological problems. Can J Earth Sci 27: 1431–1450

Parrish RR (1995) Thermal evolution of the southeastern Canadian Cordillera. Can J Earth Sci 32: 1618–1642

Podor R (1995) Raman spectra of the actinide-bearing monazites. Eur J Mineral 7: 1353–1360

Salje EKH (2000) Structural transformations in minerals: the role of temperature and radiation damage. Ber Deutschen Mineralogischen Gesellschaft, Beihefte Eur J Mineral 12: 175

Salje EKH, Chrosch J, Ewing RC (1999) Is "metamictization" of zircon a phase transition? Am Mineral 84: 1107–1116

Schärer U, Xu RH, Allègre CJ (1986) U–(Th)–Pb systematics and ages of Himalayan leucogranites, South Tibet. Earth Plan Sci Lett 77: 35–48

Seydoux AM, Montel JM, Paquette JL, Marinho M (1999) Experimental study of the resetting of the U–Th–Pb geochronological system of monazite. EUG X, Terra Nova 10, Abstr Suppl 1: 800

Seydoux AM, Wirth R, Montel JM, Heinrich W (2000) Why is monazite rarely metamict? An experimental and HR-TEM study of its annealing. Ber Deut Mineralogischen Ges, Beihefte Eur J Mineral 12: 196

Smith HA, Barreiro B (1990) Monazite U–Pb dating of staurolite grade metamorphism in pelitic schists. Contrib Mineral Petrol 105: 602–615

Smith HA, Giletti BJ (1997) Lead diffusion in monazite. Geochim Cosmochim Acta 61: 1047–1055

Speer JA (1982) Zircon. In: Reviews in mineralogy, vol. 5. Ribbe PH (ed) Mineralogical Society of America, Washington DC, pp 67–112

Suzuki K, Adachi M, Kajizuka I (1994) Electron microprobe observations of Pb diffusion in metamorphosed detrital monazites. Earth Plan Sci Lett 128: 391–405

Teufel S, Heinrich W (1997) Partial resetting of the U–Pb isotope system in monazite through hydrothermal experiments: an SEM and U–Pb isotope study. Chem Geol 137: 273–281

Weber WJ, Ewing RC, Wang LM (1994) The radiation-induced crystalline-to-amorphous transition in zircon. J Mater Res 9: 688–698

Weber WJ, Ewing RC, Catlow CRA, Diaz de la Rubia T, Hobbs LW, Kinishita C, Matzke HJ, Motta AT, Nastasi M, Salje EHK, Vance ER, Zinkle SJ (1998) Radiation effects in crystalline ceramics for the immobilization of high-level nuclear waste and plutonium. J Mater Res 13: 1434–1484

Zhang LS, Schärer U (1996) Inherited Pb components in magmatic titanite and their consequence for the interpretation of U–Pb ages. Earth Plan Sci Lett 138: 57–65